https://doi.org/10.18321/1104

Processing Conditions Optimization for the Synthesis and Consolidation of High-Entropy Diborides

S. Barbarossa, M. Murgia, R. Orrù*, G. Cao

Dipartimento di Ingegneria Meccanica, Chimica, e dei Materiali, Unità di Ricerca del Consorzio Interuniversitario Nazionale per la Scienza e Tecnologia dei Materiali (INSTM), Università degli Studi di Cagliari, via Marengo 2, 09123 Cagliari, Italy

This paper is devoted to the celebration of 75 years' jubilee of Professor Zulkhair Mansurov.
One of the authors (Roberto Orrù) would like to acknowledge Zulkhair Mansurov for his vigorous effort given for the development and diffusion of the Eurasian Chemico-Technological Journal.

Article info

Received:
9 February 2021

Received in revised form:
23 April 2021

Accepted:
15 June 2021

Keywords:
UHTCs
HEBs
Oxides
Graphite
SPS
SHS

Abstract

The fabrication by Spark Plasma Sintering (SPS) of bulk high entropy ceramics from powders obtained by Self-propagating High temperature Synthesis (SHS) is addressed in this work. The effect produced by the introduction of 1 wt.% of graphite to the powders before SPS is investigated under different temperature conditions. The final density and composition of sintered $(Hf_{0.2}Mo_{0.2}Zr_{0.2}Ti_{0.2}Ta_{0.2})B_2$ and $(Hf_{0.2}Mo_{0.2}Zr_{0.2}Ti_{0.2}Nb_{0.2})B_2$ ceramics are found to be negatively affected by the presence of oxide impurities in the powders. While product composition can be progressively improved when the temperature is increased from 1800 to 1950 °C, residual porosities remain relatively high if using additive-free powders. In contrast, the introduction of 1 wt.%C markedly allows for oxides elimination by carbothermal reduction mechanism. Products consolidation is correspondingly enhanced so that relative densities of about 97% are attained. Other than the latter effect, surface oxides removal also makes powders more reactive, thus the synthesis of single-phase products is promoted. In particular, fully homogeneous $(Hf_{0.2}Mo_{0.2}Zr_{0.2}Ti_{0.2}Ta_{0.2})B_2$ ceramics are obtained at relatively lower temperature conditions (1850 °C).

1. Introduction

Ultra-High Temperature Ceramics (UHTCs) based on transition metal borides, carbides, nitrides, carbonitrides, etc., possess a combination of desirable chemico-physical and mechanical properties (melting point above 3000 °C, high hardness, low density, chemical inertness, good electrical and thermal conductivity, low neutron absorption, selective solar energy absorption, etc.) which makes them candidate materials to operate under severe environments like in the aerospace as well as other innovative and traditional fields [1–5]. Such potential promoted a significant effort by several research groups in the last two decades to: a) identify suitable synthesis/consolidation methods for the obtainment of various members of this materials family, and b) characterize in detail the resulting products. In this context, the studies carried out so far involve mostly individual borides (ZrB_2, HfB_2, TaB_2, TiB_2, etc.) and carbides (ZrC, HfC, TaC, TiC, etc.), also used in combination with some additives (SiC, $MoSi_2$, $HfSi_2$, fiber/whisker reinforcements, etc.) to improve their properties [1–3, 6–10]. Binary solid solutions, such as $(Zr,Ta)B_2$ and $(Hf,Ta)B_2$, have been also investigated [11–13].

More recently, a novel subclass of UHTCs, known as High Entropy Borides (HEBs), has been developed [14–30]. According to the general definition of high-entropy alloys [31], HEBs consist

*Corresponding author.
E-mail: roberto.orru@dimcm.unica.it

of typically four-five transition metal cations homogeneously distributed in near-equiatomic percentage into the diboride lattice, to generate single-phase crystalline solid solutions, which are thermodynamically stable and display maximum configurational entropy. Examples of these ceramics are $(Hf_{0.2}Nb_{0.2}Zr_{0.2}Mo_{0.2}Ti_{0.2})B_2$, $(Hf_{0.2}Mo_{0.2}Zr_{0.2}Ti_{0.2}Ta_{0.2})B_2$, $(Hf_{0.2}Mo_{0.2}Zr_{0.2}Ti_{0.2}Nb_{0.2})B_2$, etc. As for their fabrication in bulk form, Spark Plasma Sintering (SPS) is the main consolidation technology utilized to this aim [14–29]. On the other hand, different approaches are proposed to synthesize the corresponding powders. The most widely employed routes are based on the borothermal or boro-carbothermal reduction of metal oxides [17–18, 20, 26–29]. Alternatively, the co-milling of individual borides [14, 22] and the self-propagating high temperature synthesis (SHS) from elemental constituents [15–16, 24–25] are adopted instead. In this regard, even if SHS did not lead to single phase high entropy products, it allowed for the fast (order of seconds) obtainment of multiphase ceramics, with elemental metals well mixed across each grain [15–16, 24–25]. The latter feature is extremely important to promote the formation of a single-phase product when SHS powders are processed by SPS. Another important aspect to be mentioned is related to the effect produced by the addition of small amounts of graphite to SHS powders prior sintering [24]. The use of this additive is aimed to reduce/eliminate oxide impurities often found in the raw powders or formed during the synthesis process [14, 19, 24, 27]. O-contamination in metal borides represents a critical issue as it hinders their consolidation. When these impurities are present, grain coarsening is promoted through evaporation–condensation mechanism, so that the driving force for densification is consequently diminished [32–34]. For instance, depending upon the HEB system, oxides content in the range 2–9 wt.% were found to correspond to 88.0–92.5% dense products obtained by SPS at 1950 °C (20 min, 20 MPa) from SHS powders [24]. Similarly, residual oxides were also found in powders obtained using borothermal and boro-carbothermal reduction routes [26, 30].

A systematic study relative to the effect induced by the introduction of 0.5 to 10 wt.% of graphite to the SHS powders evidenced that small amounts of this additive (0.5–1.0 wt.%) markedly purifies the ceramics during SPS, with a significant abatement of the oxide content (0.2–0.5 wt.%) and concurrent improvement of powder consolidation (approximately 97% of their theoretical values) [24]. Relative density is slightly enhanced (98–99%) as the graphite amount is further increased, with no additional oxides removal. Finally, the optimal amount of graphite to minimize oxide impurities was found to be 1.0 wt.%. It should be noted that all the SPS experiments involved in the latter investigation were conducted at 1950 °C.

Therefore, to complete the optimization of the processing conditions to obtain homogeneous and nearly full dense HEBs, the effect of the dwell temperature is systematically investigated for the first time in this work when considering the $(Hf_{0.2}Mo_{0.2}Zr_{0.2}Ti_{0.2}Ta_{0.2})B_2$ and $(Hf_{0.2}Mo_{0.2}Zr_{0.2}Ti_{0.2}Nb_{0.2})B_2$ systems. This study is carried out either with no graphite or in presence of 1 wt.% of additive. Detailed XRD and SEM-EDS analyses are performed on the corresponding SPS products to identify the milder conditions required to achieve a homogeneous and single-phase product.

2. Experimental

The synthesis of $(Hf_{0.2}Mo_{0.2}Zr_{0.2}Ti_{0.2}Ta_{0.2})B_2$ and $(Hf_{0.2}Mo_{0.2}Zr_{0.2}Ti_{0.2}Nb_{0.2})B_2$, hereto after also indicated as S1 and S2 for the sake of brevity, was carried out using the commercial powders listed in Table.

Precursors were first dry mixed for 20 min using a SPEX 8000 (SPEX CertiPrep, USA) shaker mill, plastic flasks, and alumina balls, according to the following stoichiometries:

$$0.2Hf + 0.2Mo + 0.2Zr + 0.2Ti + 0.2Ta + 2.2B \rightarrow (Hf_{0.2}Mo_{0.2}Zr_{0.2}Ti_{0.2}Ta_{0.2})B_2 \quad (1)$$

$$0.2Hf + 0.2Mo + 0.2Zr + 0.2Ti + 0.2Nb + 2.2B \rightarrow (Hf_{0.2}Mo_{0.2}Zr_{0.2}Ti_{0.2}Nb_{0.2})B_2 \quad (2)$$

The used boron/metal ratio overcomes the stoichiometric value in Eqs. (1) and (2), i.e. 2.2 instead of 2. Indeed, as explained elsewhere [9], the high-temperature conditions encountered during the SHS process for the synthesis of metal diborides leads to volatilization phenomena, also caused by the borothermal reduction of oxide impurities in raw powders, which determine some extra boron consumption.

Cylindrical pellets obtained by uniaxially pressing the starting mixture were reacted by SHS under Argon environment. The resulting powders were used for consolidation purposes either with no additive or once combined with 1.0 wt.% graphite

Table
Raw powders used for the preparation of High Entropy Diborides

Reactant	Vendor	Particle size (μm)	Purity (%)
Hf	Alfa Aesar, cod. 10201	< 44	99.6
Mo	Alfa Aesar, cod. 10031	< 149	99.95
Nb	Alfa Aesar, cod. 10275	< 44	99.8
Ta	Alfa Aesar, cod. 00337	< 44	99.9
Ti	Aldrich, cod. 26.849-6	< 149	99.7
Zr	Alfa Aesar, cod. 00418	< 44	>99.5
B, amorphous	Aldrich, cod.15580	-	≥ 95
C, graphite	Aldrich, cod. 28286-3	< 20	-

(Table). Both systems underwent a ball milling treatment (60 min, ball to powder weight ratio equal to 2) using a SPEX 8000 (SPEX CertiPrep, USA) equipped with stainless steel vial and four steel balls (approximately 4.5 g, 10 mm diameter).

Bulk samples (14.7 mm diameter, 2.5–3.5 mm height) were obtained by SPS (515S model equipment, Fuji Electronic Industrial Co., Ltd., Kanagawa, Japan) under vacuum conditions (about 20 Pa). During the sintering process, the temperature was measured and controlled by an infrared pyrometer (CHINO, mod. IR-AHS2, Japan) focused on the external surface of a cylindrical mould (30 mm external diameter; 15 mm inside diameter; 30 mm height) made of AT101 graphite (ATAL Srl, Italy). Additional general details of the SPS procedure can be found elsewhere [24]. In the present work, during sintering experiments, the temperature was increased from the room to the dwell (T_D) level at a constant rate (200 °C/min), followed by a holding period at t_D of 20 min duration and, finally, a cooling step. The applied pressure was kept constant to 20 MPa for the entire process. The effect of the SPS temperature was investigated in the range 1800–1950 °C. Each experiment was repeated at least twice, for the sake of reproducibility.

Samples density was measured by Archimedes' method using distilled water as an immersion medium. Relative densities of $(Hf_{0.2}Mo_{0.2}Zr_{0.2}Ti_{0.2}Ta_{0.2})B_2$ and $(Hf_{0.2}Mo_{0.2}Zr_{0.2}Ti_{0.2}Nb_{0.2})B_2$ SPS products were calculated by considering their theoretical values of 8.52 and 7.37 g/cm^3, respectively [14]. When graphite was combined with SHS powders, its presence was properly taken into account for evaluating the relative densities of the resulting composite systems [35]. To this aim, the value of 2.26 g/cm^3 was used for this additive [36].

Products composition was determined by X-ray diffraction analysis (Philips PW 1830, Netherlands) using Cu Kα radiation, generally over a range of scattering angles 2ə from 25° to 45°, in steps of 0.05° with 15 s acquisition time per angle.

The microstructure (homogeneity, residual porosity, etc.) of the cross sections of SPS samples was assessed by high resolution scanning electron microscopy (HRSEM) (mod. S4000, Hitachi, Tokyo, Japan) equipped with a UltraDry EDS Detector (Thermo Fisher Scientific, Waltham, MA, USA).

3. Results and discussion

As reported in two recent works [24–25], the synthesis of $(Hf_{0.2}Mo_{0.2}Zr_{0.2}Ti_{0.2}Ta_{0.2})B_2$ and $(Hf_{0.2}Mo_{0.2}Zr_{0.2}Ti_{0.2}Nb_{0.2})B_2$ by SHS according to Eqs. (1) and (2), respectively, did not go to completion. Specifically, when considering system S1, the synthesized powders consisted of approximately 70 wt.% of the expected high entropy ceramic, along with $(Hf_{0.5}Ti_{0.5})B_2$, $(ZrTiB_4)_{0.5}$, TaB_2, HfB_2, unreacted Mo, etc., as secondary phases [24]. A multiphase product is also formed during SHS of $(Hf_{0.2}Mo_{0.2}Zr_{0.2}Ti_{0.2}Nb_{0.2})B_2$, with the content of the desired HEB phase less than 30 wt.%, and the rest of the powders made of $(Hf_{0.5}Ti_{0.5})B_2$, $(Zr_{0.5}Ti_{0.5})B_2$, NbB_2, and other minor species [25].

SHS powders of S1 and S2 systems were subsequently processed by SPS under different dwell temperature conditions. As mentioned in the Introduction, the optimal amount of graphite to be used for minimizing oxide impurities and increasing product density at 1950 °C was recently found to be 1.0 wt.% [24]. Therefore, the influence of the sintering temperature on product microstructure is investigated in this work in presence of the latter additive percentage.

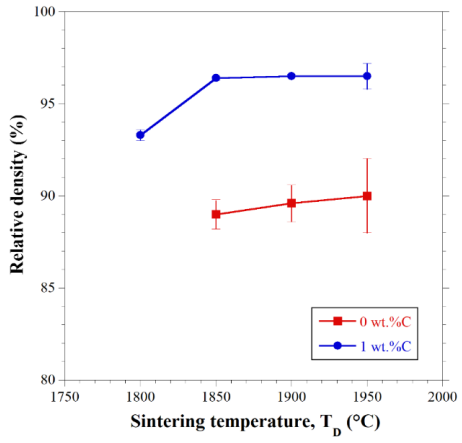

Fig. 1. Effect of dwell temperature on the densification by SPS of $(Hf_{0.2}Mo_{0.2}Zr_{0.2}Ti_{0.2}Ta_{0.2})B_2$ samples without or in presence of 1 wt.% graphite additive.

As far as the S1 system is concerned, Fig. 1 shows that average densities equal or lower than 90% of the theoretical value are achieved when the consolidation of SHS powders is carried out with no graphite. In addition, an increase of the sintering temperature from 1850 to 1950 °C provides only a modest improvement of sample densification. A significantly different behavior is observed with the addition of graphite to SHS powders. Fig. 1 shows that, in the latter case, SPS samples display higher densities, compared to those ones obtained with no additive, even when operating at relatively lower temperature levels. Moreover, when graphite is used, an increase of T_D from 1800 to 1850 °C is accompanied by a marked enhancement of powder consolidation.

The powder densification behavior described above could be readily associated with the compositional differences in the obtained products. XRD patterns of the various S1 ceramics obtained by SPS at different T_D levels, with or without graphite, are reported in Fig. 2(a)-2(b). From this analysis, it is possible to deduce that the desired high-entropy compound represents the main phase in all the SPS samples, regardless of the operating conditions adopted. Nonetheless, from the log scale spectra shown in Fig. 2(b), the presence of metal oxides, namely HfO_2, is observed in SPS samples processed with no graphite. On the other hand, such peaks disappear from XRD patterns of S1 products obtained in the range 1800–1950 °C when graphite was added to the SHS powders.

Therefore, according to previous findings [24], it is possible to state that the presence of these oxides in samples undergoing SPS unequivocally hinders their densification. Moreover, the introduction of small amounts of graphite determines the carbothermal reduction of these impurities and concurrently promotes the consolidation process. Another important issue to be considered is related to product microstructure, with particular emphasis to the distribution of metal elements across the volume sample. This aspect is very crucial since it allows one to assess if a single-phase and homogeneous product is achieved. The SEM micrographs and related EDS maps of S1 specimens obtained under the diverse operating conditions explored in this work are reported in Fig. 3(a)-3(e). First, it is confirmed that the ceramic obtained at T_D = 1850 °C with no graphite exhibits a high porosity level. In addition, the distribution of elements in the sample is significantly not uniform (Fig. 3(a)). The latter characteristic is markedly improved as the temperature is raised to 1950 °C, whereas residual porosity remains basically unchanged (Fig. 3(b)).

The use of 1 wt.% graphite provides a beneficial effect from both product densification and homogeneity points of view. This can be readily observed even when operating at relatively lower temperatures, for instance 1800 °C (Fig. 3(c)). Indeed, a considerable consolidation improvement, as well as an enhancement of elements distribution across the sample, can be correspondingly observed. However, product homogeneity is satisfying only when T_D is further increased to 1850 °C, which also leads to denser ceramics (Fig. 3(d)). No additional benefits in sample microstructure are found when the temperature is raised to 1950 °C (Fig. 3(e)), except for sample porosity

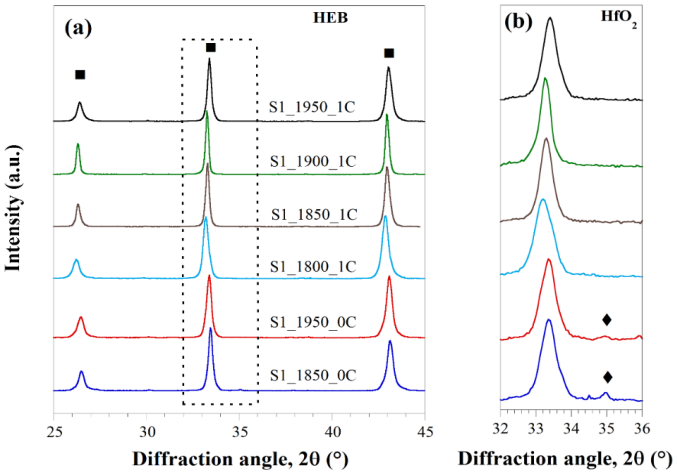

Fig. 2. XRD patterns relative to $(Hf_{0.2}Mo_{0.2}Zr_{0.2}Ti_{0.2}Ta_{0.2})B_2$ samples obtained at different temperatures by SPS without or in presence of graphite additive: (a) complete and (b) detailed spectra on a log scale.

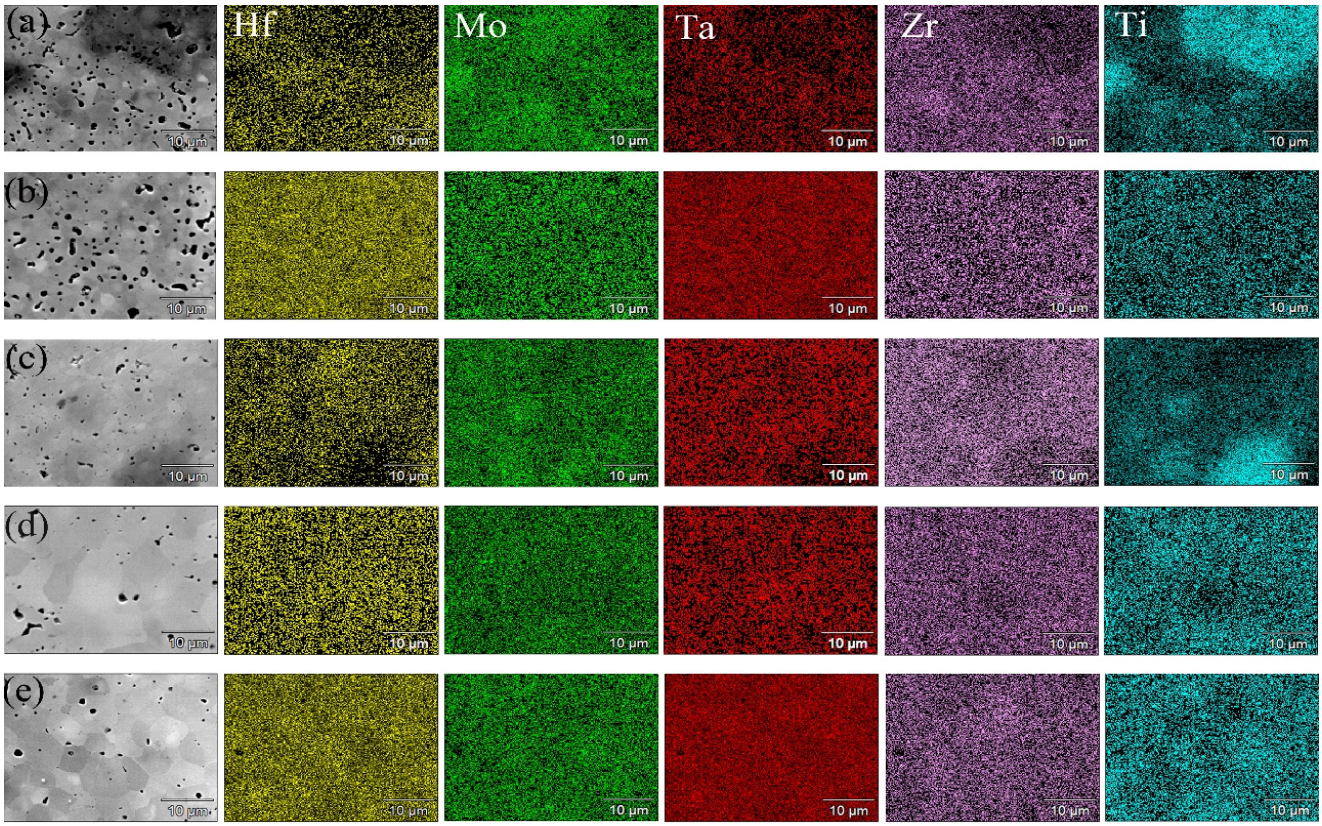

Fig. 3. Cross sectional SEM micrographs and corresponding EDS elemental maps of the $(Hf_{0.2}Mo_{0.2}Zr_{0.2}Ti_{0.2}Ta_{0.2})B_2$ samples obtained by SPS: (a) –1850 °C/0 wt.%C; (b) – 1950 °C/0 wt.%C; (c) – 1800 °C/1 wt.%C; (d) – 1850 °C/1 wt.%C; (e) – 1950 °C/1 wt.%C.

which is further reduced. Based on the results described above, it is possible to conclude that the introduction of 1 wt.% graphite not only facilitates the densification of SHS powders by SPS, but also determines a decrease of the sintering temperature required for completing the chemical transformation to the desired $(Hf_{0.2}Mo_{0.2}Zr_{0.2}Ti_{0.2}Ta_{0.2})B_2$ ceramic. In particular, the latter target is reached in this work at T_D = 1850 °C, i.e. 100 °C below with respect to the condition explored in our previous study [24].

Let us now consider the second high-entropy system investigated in this work, i.e. $(Hf_{0.2}Mo_{0.2}Zr_{0.2}Ti_{0.2}Nb_{0.2})B_2$. Similarly to the S1 system, the consolidation by SPS of additive free SHS powders when T_D = 1850 °C leads to a bulk product only 90% dense, as shown in Fig. 4.

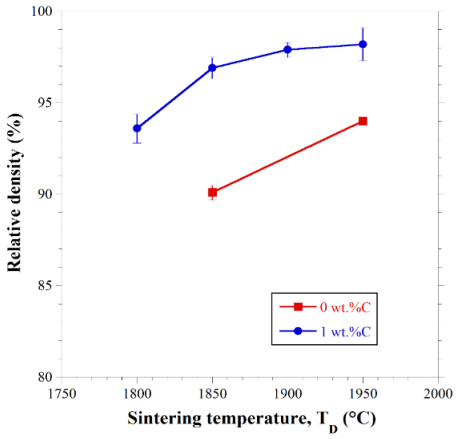

Fig. 4. Effect of dwell temperature on the densification by SPS of $(Hf_{0.2}Mo_{0.2}Zr_{0.2}Ti_{0.2}Nb_{0.2})B_2$ samples without or in presence of 1 wt.% graphite additive.

The XRD analysis of the latter sample indicates, other than the main desired phase, also the presence of oxides impurities (Fig. 5). An increase of the temperature to 1950 °C is certainly beneficial but the resulting ceramic still has an inadequate relative density (about 94%). As for S1 system, the introduction of graphite leads to the elimination of HfO_2 (Fig. 5) and, in parallel, a marked improvement of powders consolidation. Densities equal or exceeding 97% of the theoretical value are achieved when operating at 1850 °C or higher temperatures.

The micrographs shown in Fig. 6 along with the corresponding EDS maps provide a clear indication of products microstructure. Without the contribution of graphite, a porous and non-homogeneous ceramic is obtained at 1850 °C (Fig. 6a).

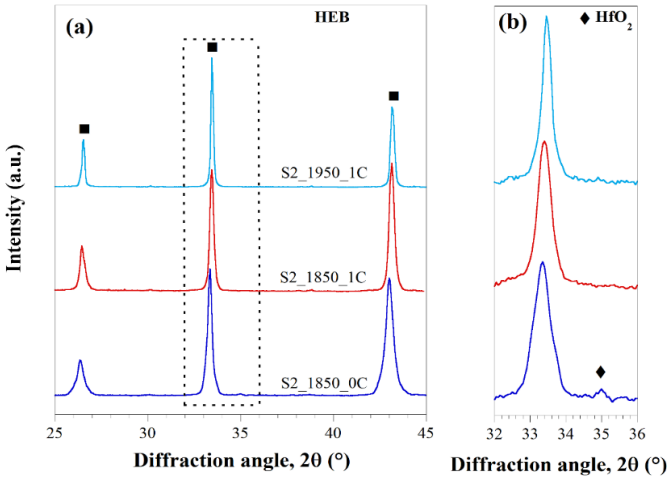

Fig. 5. XRD patterns relative to ($Hf_{0.2}Mo_{0.2}Zr_{0.2}Ti_{0.2}Nb_{0.2}$)$B_2$ samples obtained at different temperatures by SPS without or in presence of graphite additive: (a) complete and (b) detailed spectra on a log scale.

These characteristics are both improved with an increase of the temperature to 1950 °C (Fig. 6b). Nonetheless, product densification is still not satisfactory and Nb and Mo are not uniformly distributed across the sample. With the introduction of graphite, denser samples are produced by SPS at 1850 °C, whereas material homogeneity is still scarce (Fig. 6c). An increase of the temperature to 1900 °C is beneficial for both these characteristics, but the uniform distribution of the five metals is not reached (Fig. 6d). In contrast, Fig. 6e shows that the target is fully achieved when the SHS powders containing 1 wt.% graphite are processed at 1950 °C. Correspondingly, an almost fully dense and perfectly homogeneous ceramic is produced.

Based on the results described above, it is possible to state that, when processing additive-free SHS powders, a homogeneous distribution of elemental constituents can be achieved by SPS only if a dwell temperature of 1950 °C is adopted. Nevertheless, the resulting ceramic is rather porous. The latter drawback is apparently caused by the presence of oxide impurities in SHS powders, which are known to hamper their densification. However, the use of 1 wt.% of graphite allows for the removal of such oxides by carbothermal reduction mechanism. A clear increase of product densification is correspondingly observed. The present study also evidenced that the elimination of oxide contaminants from particles surface gives rise to an additional beneficial effect,

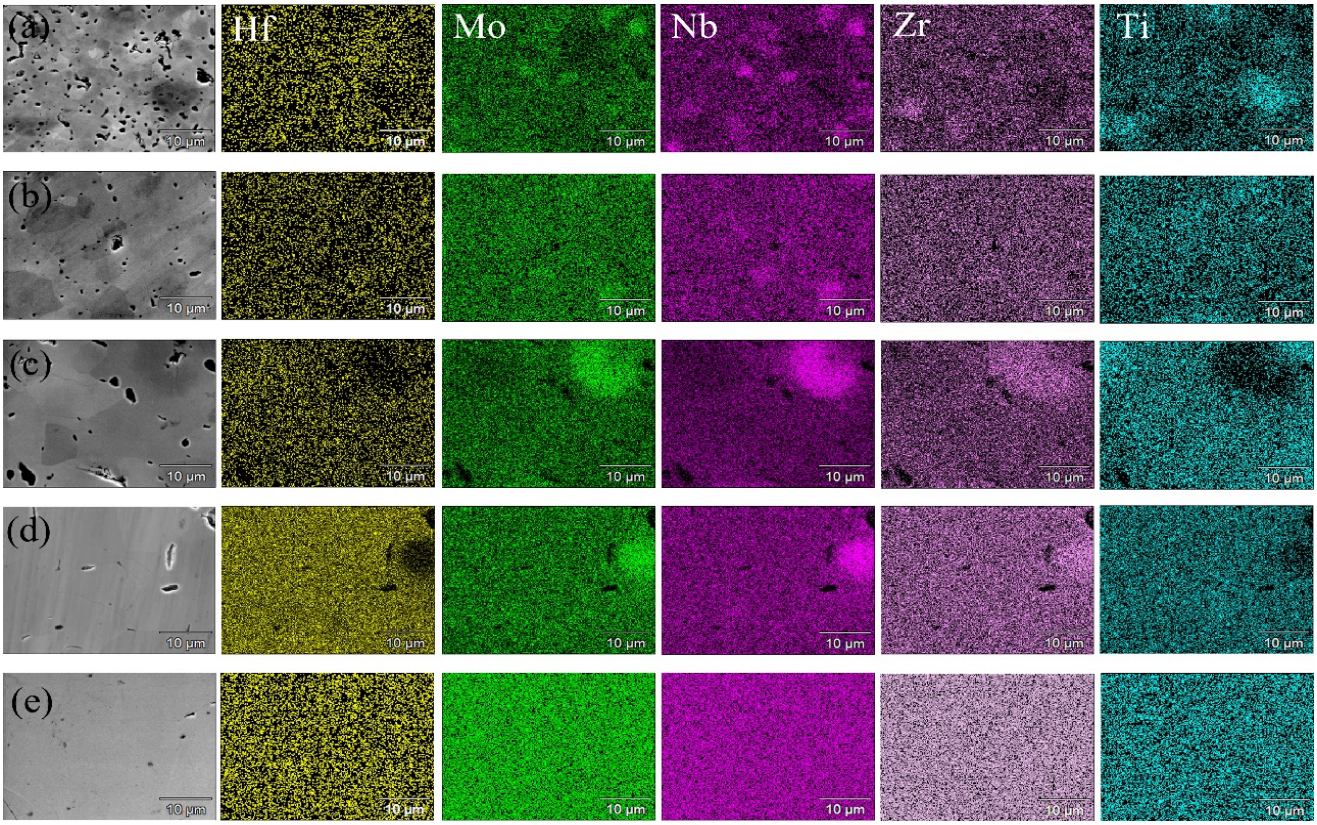

Fig. 6. Cross sectional SEM micrographs and corresponding EDS elemental maps of the ($Hf_{0.2}Mo_{0.2}Zr_{0.2}Ti_{0.2}Nb_{0.2}$)$B_2$ samples obtained by SPS: (a) – 1850 °C/0 wt.%C; (b) – 1950 °C/0 wt.%C; (c) – 1850 °C/1 wt.%C; (d) – 1900 °C/1 wt.%C; (e) – 1950 °C/1 wt.%C.

i.e. the improved powder reactivity. This feature was unequivocally observed when considering the $(Hf_{0.2}Mo_{0.2}Zr_{0.2}Ti_{0.2}Ta_{0.2})B_2$ system. Indeed, while Fig. 3a shows that a non-homogeneous and porous ceramic is obtained at 1850 °C with no graphite, the same SPS conditions applied in presence of 1 wt.%C lead to a single phase and nearly full dense high entropy ceramic. Therefore, the consequences deriving from the introduction of some graphite cannot be only confined to powder densification improvement achieved during SPS but are also related to the increased conversion rate to the desired high-entropy phase.

4. Conclusions

The effect of the sintering temperature on product composition and densification behavior during the fabrication by SPS of bulk $(Hf_{0.2}Mo_{0.2}Zr_{0.2}Ti_{0.2}Ta_{0.2})B_2$ and $(Hf_{0.2}Mo_{0.2}Zr_{0.2}Ti_{0.2}Nb_{0.2})B_2$ from SHS powders is systematically investigated in this work. The consolidation of as synthesized powders is significantly hindered by the presence of oxides impurities. Indeed, the corresponding sintered ceramics display high residual porosities, even when the temperature is increased up to 1950 °C. Such contaminants can be markedly removed by carbothermal reduction mechanism, through the addition of a small amount (1 wt.%) of graphite to the SHS powders prior SPS. This outcome is also accompanied, for both high entropy systems, by a significant improvement of the relative density of sintered products. Furthermore, the removal of surface oxides by graphite makes powders undergoing SPS more reactive. This fact determines not only the enhanced powders sinterability mentioned above, but also promotes the obtainment of single-phase products during SPS. In particular, for the case of $(Hf_{0.2}Mo_{0.2}Zr_{0.2}Ti_{0.2}Ta_{0.2})B_2$, the present study evidenced that highly dense and fully homogeneous ceramics can be obtained at lower temperature conditions compared to those ones adopted previously [24], i.e. 1850 °C instead of 1950 °C. On the other hand, the latter condition was anyway required to achieve the same goal when considering the $(Hf_{0.2}Mo_{0.2}Zr_{0.2}Ti_{0.2}Nb_{0.2})B_2$ system.

In conclusion, the combination of the SHS and SPS methods provides, along with the use of small amounts of graphite as additive, a valuable and rapid tool for the fabrication of dense and pure high-entropy borides. This approach could be readily extended also for the obtainment of other high entropy ceramics in bulk form.

Acknowledgements

The present work has been carried out in the framework of the ARCHIMEDES project sponsored by Regione Autonoma della Sardegna (Italy) – Fondo di Sviluppo e Coesione (FSC) 2014-2020 (Cod. RAS: RASSR88309, Cod. CUP: F76C18000980002). One of the authors (S.B.) performed his activity in the framework of the International PhD in Innovation Sciences and Technologies at the University of Cagliari, Italy. One of us (G.C.) acknowledges the results obtained in this manuscript as quite important for the "Ithermal" and "Generazione E" projects, sponsored by Sardegna Ricerche, Italy (Cod. CUP: F21I18000130006) and by the Italian Ministry of Education, University and Research, Italy (Cod. CUP: B96G18000560005), respectively. Thanks are due to Mr. Daniele Lai and Mr. Gianluca Marongiu (University of Cagliari) for their technical assistance. The contribution of Dr. Sebastiano Garroni and Antonio Iacomini (University of Sassari, Italy) is also gratefully acknowledged.

References

[1]. W.G. Fahrenholtz, G.E. Hilmas, *Scripta Mater.* 129 (2017) 94–99. DOI: 10.1016/j.scriptamat.2016.10.018

[2]. R. Orrù, G. Cao, Ultra-high temperature ceramics by spark plasma sintering. In Spark Plasma Sintering: Current Status, New Developments and Challenges (Eds.: G. Cao, C. Estournés, J. Garay, R. Orrù), 2019, p. 49–76. DOI: 10.1016/B978-0-12-817744-0.00002-7

[3]. B.R. Golla, A. Mukhopadhyay, B. Basu, S.K. Thimmappa, *Prog. Mater. Sci.* 111 (2020) 100651. DOI: 10.1016/j.pmatsci.2020.100651

[4]. E. Sani, L. Mercatelli, M. Meucci, A. Balbo, C. Musa, R. Licheri, R. Orrù, G. Cao, *Renew. Energ.* 91 (2016) 340–346. DOI: 10.1016/j.renene.2016.01.068

[5]. V.S. Buinevich, A.A. Nepapushev, D.O. Moskovskikh, G.V. Trusov, K.V. Kuskov S.G. Vadchenko A.S. Rogachev, A.S Mukasyan, *Ceram. Int.* 46 (2020) 16068–16073. DOI: 10.1016/j.ceramint.2020.03.158

[6]. D. Chen, L. Xu, X. Zhang, B. Ma, P. Hu, *Int. J. Refract. Met. Hard Mater.* 27 (2009) 792–795. DOI: 10.1016/j.ijrmhm.2009.01.002

[7]. P. Zhang, P. Hu, X. Zhang, J. Han, S. Meng, *J. Alloys Compd.* 472 (2009) 358–362. DOI: 10.1016/j.jallcom.2008.04.082

[8]. C. Musa, R. Licheri, R. Orrù, G. Cao, *Eurasian Chem-Technol. J.* 15 (2013) 117–126. DOI: 10.18321/ectj149

[9]. C. Musa, R. Orrù, D. Sciti, L. Silvestroni, G. Cao, *J. Eur. Ceram. Soc.* 33 (2013) 603–614. DOI: 10.1016/j.jeurceramsoc.2012.10.004
[10]. C. Musa, R. Licheri, R. Orrù, G. Cao, *Ind. Eng. Chem. Res.* 53 (2014) 9101–9108. DOI: 10.1021/ie4032692
[11]. V.V. Kurbatkina, E.I. Patsera, E.A. Levashov, A.N. Timofeev, *J. Eur. Ceram. Soc.* 38 (2018) 1118–1127. DOI: 10.1016/j.jeurceramsoc.2017.12.031
[12]. V.V. Kurbatkina, E.I. Patsera, E.A. Levashov, *Ceram. Int.* 45 (2019) 4067–4075. DOI: 10.1016/j.ceramint.2018.10.113
[13]. V.V. Kurbatkina, E.I. Patsera, D.V. Smirnov, E.A. Levashov, S. Vorotilo, A.N. Timofeev, *Ceram. Int.* 45 (2019) 4076–4083. DOI: 10.1016/j.ceramint.2018.10.165
[14]. J. Gild, Y. Zhang, T. Harrington, S. Jiang, T. Hu, M.C. Quinn, W.M. Mellor, N. Zhou, K. Vecchio, J. Luo, *Sci. Rep.* 6 (2016) 37946. DOI: 10.1038/srep37946
[15]. G. Tallarita, R. Licheri, S. Garroni, R. Orrù, G. Cao, *Scripta Mater.* 158 (2019) 100–104. DOI: 10.1016/j.scriptamat.2018.08.039
[16]. G. Tallarita, R. Licheri, S. Garroni, S. Barbarossa, R. Orrù, G. Cao, *J. Eur. Ceram. Soc.* 40 (2020) 942–952. DOI: 10.1016/j.jeurceramsoc.2019.10.031
[17]. L. Feng, W.G. Fahrenholtz, G.E. Hilmas, *J. Eur. Ceram. Soc.* 40 (2020) 3815–3823. DOI: 10.1016/j.jeurceramsoc.2020.03.065
[18]. L. Feng, W.G. Fahrenholtz, G.E. Hilmas, F. Monteverde, *J. Eur. Ceram. Soc.* 41 (2021) 92–100. DOI: 10.1016/j.jeurceramsoc.2020.08.058
[19]. J. Gild, K. Kaufmann, K. Vecchio, J. Luo, *Scripta Mater.* 170 (2019) 106–110. DOI: 10.1016/j.scriptamat.2019.05.039
[20]. J. Gild, A. Wright, K. Quiambao-Tomko, M. Qin, J.A. Tomko, M Shafkat bin Hoque, J.L. Braun, B. Bloomfield, D. Martinez, T. Harrington, K. Vecchio, P.E. Hopkins, J. Luo, *Ceram. Int.* 46 (2020) 6906–6913. DOI: 10.1016/j.ceramint.2019.11.186
[21]. J.F. Gu, J. Zou, S. K. Sun, H. Wang, S.Y. Yu, J. Zhang, W. Wang, Z. Fu, *Sci. China Mater.* 62 (2019) 1898–1909. DOI: 10.1007/s40843-019-9469-4
[22]. M. Qin, J. Gild, C. Hu, H. Wang, M.S.B. Hoque, J.L. Braun, T.J. Harrington, P.E. Hopkins, K.S. Vecchio, J. Luo, *J. Eur. Ceram. Soc.* 40 (2020) 5037–5050. DOI: 10.1016/j.jeurceramsoc.2020.05.040
[23]. M. Qin, J. Gild, H. Wang, T.J. Harrington, K.S. Vecchio, J. Luo, *J. Eur. Ceram. Soc.* 40 (2020) 4348–4353. DOI: 10.1016/j.jeurceramsoc.2020.03.063
[24]. S. Barbarossa, R. Orrù, S. Garroni, R. Licheri, G. Cao, *Ceram. Int.* 47 (2021) 6220–6231. DOI: 10.1016/j.ceramint.2020.10.200
[25]. S. Barbarossa, R. Orrù, V. Cannillo, A. Iacomini, S. Garroni, M. Murgia, G. Cao, *Ceramics* 4 (2021) 108–120. DOI: 10.3390/ceramics4020010
[26]. Y. Zhang, W.M. Guo, Z.B. Jiang, Q.Q. Zhu, S.K. Sun, Y. You, K. Plucknett, H.T. Lin, *Scripta Mater.* 164 (2019) 135–139. DOI: 10.1016/j.scriptamat.2019.01.021
[27]. Y. Zhang, Z.B. Jiang, S.K. Sun, W.M. Guo, Q.S. Chen, J.X. Qiu, K. Plucknett, H.T. Lin, *J. Eur. Ceram. Soc.* 39 (2019) 3920–3924. DOI: 10.1016/j.jeurceramsoc.2019.05.017
[28]. Y. Zhang, S.K. Sun, W. Zhang, Y. You, W.M. Guo, Z.W. Chen, J.H. Yuan, H.T. Lin, *Ceram. Int.* 46 (2020) 14299–14303. DOI: 10.1016/j.ceramint.2020.02.214
[29]. Y. Zhang, S. K. Sun, W. M. Guo, W. Zhang, L. Xu, J. H. Yuan, D. K. Guan, D. W. Wang, Y. You, H. T. Lin, *J. Eur. Ceram. Soc.* 41 (2021) 1015–1019. DOI: 10.1016/j.jeurceramsoc.2020.08.071
[30]. J.-X. Liu, X.-Q. Shen, Y. Wu, F. Li, Y. Liang, G.-J. Zhang, *J. Adv. Ceram.* 9 (2020) 503–510. DOI: 10.1007/s40145-020-0383-8
[31]. M.-H. Tsai, J.-W. Yeh, *Mater. Res. Lett.* 2 (2014) 107–123. DOI:10.1080/21663831.2014.912690
[32]. S. Baik, P.F. Becher, *J. Am. Ceram. Soc.* 70 (1987) 527–530. DOI: 10.1111/j.1151-2916.1987.tb05699.x
[33]. W.G. Fahrenholtz, G.E. Hilmas, S.C. Zhang, S. Zhu, *J. Am. Ceram. Soc.* 91 (2008) 1398–1404. DOI: 10.1111/j.1551-2916.2007.02169.x
[34]. S.K. Mishra, L.C. Pathak, *J. Alloys Compd.* 465 (2008) 547–555. DOI: 10.1016/j.jallcom.2007.11.004
[35]. F.L. Matthews, R. Rawlings Composite Materials: Engineering and Science. Chapman & Hall, Great Britain; 1994. ISBN: 9781855734739
[36]. H.O. Pierson, Handbook of Carbon, Graphite, Diamonds and Fullerenes, 1994. DOI: 10.1016/B978-0-8155-1339-1.50006-2